Cell Reports
Report

Using Micromanipulation to Analyze Control of Vertebrate Meiotic Spindle Size

Jun Takagi,[1] Takeshi Itabashi,[1] Kazuya Suzuki,[1] Tarun M. Kapoor,[2] Yuta Shimamoto,[2,3] and Shin'ichi Ishiwata[1,4,*]
[1]Department of Physics, Faculty of Science and Engineering, Waseda University, 3-4-1 Okubo, Shinjuku-ku, Tokyo 169-8555, Japan
[2]Laboratory of Chemistry and Cell Biology, The Rockefeller University, 1230 York Avenue, New York, NY 10065, USA
[3]JST PRESTO, 1230 York Avenue, New York, NY 10065 USA
[4]Waseda Bioscience Research Institute in Singapore (WABIOS), 11 Biopolis Way, 05-01/02 Helios, Singapore 138667, Singapore
*Correspondence: ishiwata@waseda.jp
http://dx.doi.org/10.1016/j.celrep.2013.09.021

SUMMARY

The polymerization/depolymerization dynamics of microtubules (MTs) have been reported to contribute to control of the size and shape of spindles, but quantitative analysis of how the size and shape correlate with the amount and density of MTs in the spindle remains incomplete. Here, we measured these parameters using 3D microscopy of meiotic spindles that self-organized in *Xenopus* egg extracts and presented a simple equation describing the relationship among these parameters. To examine the validity of the equation, we cut the spindle into two fragments along the pole-to-pole axis by micromanipulation techniques that rapidly decrease the amount of MTs. The spheroidal shape spontaneously recovered within 5 min, but the size of each fragment remained small. The equation we obtained quantitatively describes how the spindle size correlates with the amount of MTs while maintaining the shape and the MT density.

INTRODUCTION

The meiotic/mitotic spindle is a microtubule (MT)-based structure that is designed to segregate chromosomes. The size of the metaphase spindle scales with the cell size except in relatively larger cell types (Hara and Kimura, 2009; Wühr et al., 2008). The regulation of MT assembly dynamics by depolymerizing motor proteins and MT-severing and -destabilizing proteins, along with a localized signal from chromosomes to nucleate MTs, has been suggested to contribute to this cell-size-independent control of the spindle size (Budde et al., 2001; Gaetz and Kapoor, 2004; Heald et al., 1996; Houghtaling et al., 2009; Kaláb et al., 2006; Loughlin et al., 2011; Mitchison et al., 2005; Ohi et al., 2007; Reber et al., 2013). For example, addition or depletion of depolymerizing kinesins decreases or increases the spindle size, respectively (Ohi et al., 2007); inhibition of katanin, an MT-severing protein, lengthens the spindle (Loughlin et al., 2011); and a gradient of RanGTP, which promotes MT nucleation and stabilization, produces spatial cues to scale spindle size (Kaláb et al., 2006). Thus, the size of the metaphase spindle can be controlled by cytoplasmic factors regulating the MT dynamics.

However, previous studies suggested that the balance of forces generated by molecular motors that induce the sliding and depolymerizing of MTs, and the distortion of the stiff MT bundle, is also related to the regulation of spindle size (Brust-Mascher et al., 2009; Burbank et al., 2007; Goshima et al., 2005; Oguchi et al., 2011; Wollman et al., 2008). Mechanically applied forces have been reported to affect MT dynamics and spindle size without changing the cytoplasmic conditions (Dumont and Mitchison, 2009; Itabashi et al., 2009; Shimamoto et al., 2011). Although these biochemical and biophysical studies indicated that MT dynamics contributes to regulation of spindle size, correlation between the amount of MTs and spindle size, particularly in response to perturbations that leave the overall biochemical composition unchanged, remains incomplete.

MT density in the spindle has been reported to be regulated by MT-severing or -destabilizing proteins such as katanin (Andersen 2000; Budde et al., 2001; McNally et al., 2006; Vernos et al., 1995). In addition to the balance of forces generated by motors and MT bundles, molecular motors such as Eg5 and dynein have been suggested to regulate spindle shape (Gaetz et al., 2006; Hara and Kimura, 2013; Merdes et al., 1996; Rubinstein et al., 2009; Sawin et al., 1992). To determine the correlation between the amount of MTs and spindle size, it is also necessary to consider the contribution of MT density and spindle shape.

Here, we performed a 3D quantitative analysis of these parameters. We used a micromanipulation technique to control the amount of MTs within a metaphase spindle without changing the molecular composition in the cytosol and quantitatively examined the correlation between the amount of MTs and the spindle size.

RESULTS AND DISCUSSION

Spindle Size Correlates with the Amount of MTs

In *Xenopus* egg extracts (Desai et al., 1999), a cell-free system, the spindle size varies from 25 to 50 μm (Figure S1A). First, we examined the relationship between the spindle size and the

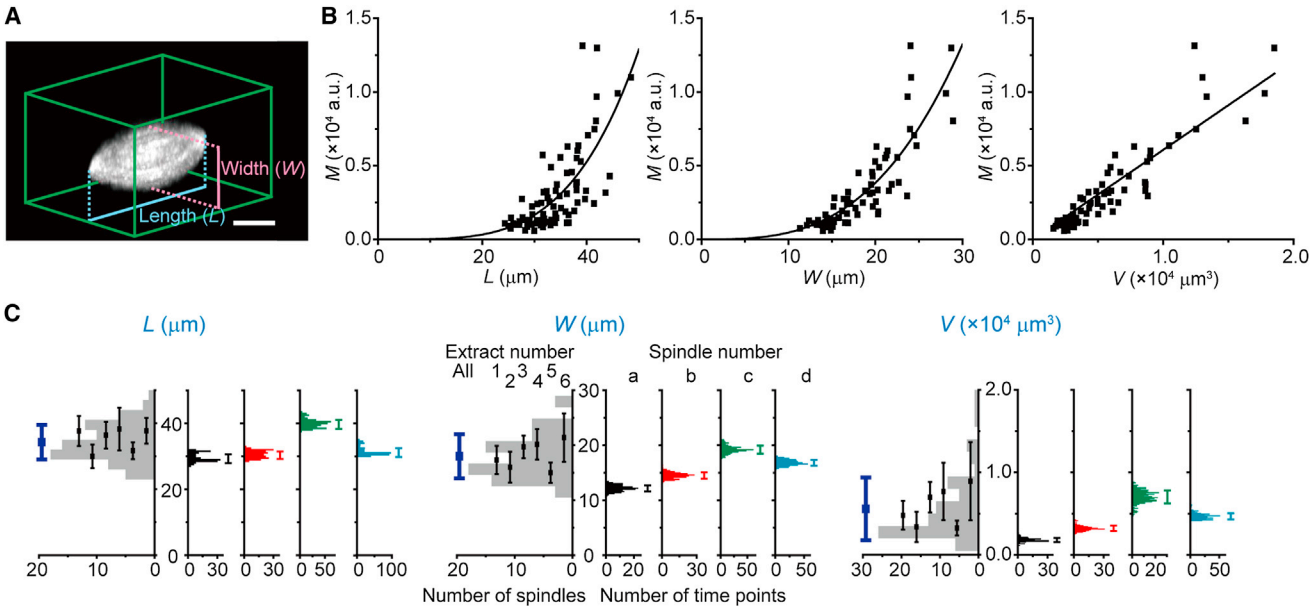

Figure 1. Correlation between Spindle Size and Amount of MTs

(A) 3D image of a metaphase spindle that self-organized in *Xenopus* egg extracts, labeled with fluorescent tubulin. 3D rendering was performed using a maximum-intensity projection technique. Scale bar, 10 μm.

(B) Relationship between spindle size (length [*L*], width [*W*], and volume [*V*]) and the amount of MTs (*M*) (n = 78 spindles). Black solid curves indicate the best fits ($M = 2.0 \times 10^{-3}\ L^{4.0}$ [$R^2 = 0.53$], $M = 4.1 \times 10^{-5}\ W^{3.1}$ [$R^2 = 0.75$], $M = 0.61 \times V$ [$R^2 = 0.93$]).

(C) Histograms on the left show the distribution of each parameter for an ensemble of 78 spindles that self-organized in six different *Xenopus* egg extracts. The thick purple bars on the left show the SD of each parameter for an ensemble of 78 spindles. The thin black bars on the left show the SD of each parameter for an ensemble of spindles in six different extracts. The histograms on the right show the distribution of each parameter within 30 min (n = 4 spindles, interval of the time lapse was 10 s [black and red] or 5 s [green and blue]). Colored bars on the right show the SD of the corresponding histograms. The values of the parameters are summarized in Table S1.

See also Figure S1A and Table S2.

amount of MTs in the spindle (*M*) using 3D observation (Figures 1A and 1B). We characterized the spindle size according to the length (*L*) as the pole-to-pole distance, the width (*W*) as the width perpendicular to the pole-to-pole axis, and the volume (*V*). The value of *M* was estimated from the fluorescence intensity (*FI*) of fluorescent-dye-labeled tubulin, which was incorporated into the spindle MTs (see Experimental Procedures for details). The average spindle *L*, *W*, and *V* values obtained for the self-organized spindles were 34.1 ± 5.3 μm, 18.0 ± 4.0 μm, and (5.56 ± 3.81) × 10^3 μm^3 (mean ± SD, n = 78 spindles), respectively. *L* and *W* had a linear relationship (Figure S1A; $W = -0.57\ L - 1.3$, Pearson correlation coefficient; r = 0.74, $p < 0.05$), and *V* was almost proportional to the cube of *L* (Figure S1A; $V = 0.035\ L^{3.4}$). We found that the spindle size correlated with the amount of MTs (*M*) (Figure 1B; n = 78 spindles, $M = [2.0 \pm 3.2] \times 10^{-3}\ L^{4.0 \pm 0.4}$ [$R^2 = 0.53$], $M = [4.1 \pm 2.7] \times 10^{-5}\ W^{3.1 \pm 0.2}$ [$R^2 = 0.75$], $M = [0.61 \pm 0.02] \times V$ [$R^2 = 0.93$]; ± SEM, black solid curves).

To examine whether the difference in the size of the spindles was derived from the intrinsic size or the time variation of each spindle, we performed time-lapse observation for 30 min using 2D observation (Figure 1C; n = 4 spindles). The spindle size fluctuated and had a single-peaked distribution (Figure 1C, histograms on the right). The standard time variation of the spindle size for each spindle (Figure 1C, bars on the right histograms) was much smaller than the SD not only for an ensemble of 78 spindles that self-organized in six different egg extracts (Figure 1C, thick purple bars on the left histogram) but also for an ensemble of spindles that self-organized in the same extract (Figure 1C, thin black bars on the left histograms; Table S1). The relationship between the spindle size and the amount of MTs suggests that each spindle has an intrinsic size and amount of MTs.

Spindle Shape and MT Density Are Determined Independently of the Spindle Length

Next, we examined the relationship between the spindle size and shape using 3D observation (Figures 2A, S1B, and S1C; correlations among the parameters are summarized in Table S2). We characterized the spindle shape according to the aspect ratio α (= *W*/*L*) and γ (= V/LW^2) and found that α and γ were maintained almost constant, independently of the spindle length (*L*) (Figure 2A; n = 78 spindles, Pearson correlation coefficient; r = 0.057 [$p > 0.05$], 0.337 [$p < 0.01$], respectively, $\alpha = 0.53 \pm 0.08$, $\gamma = 0.44 \pm 0.06$ [mean ± SD]), and that the 3D spindle shape was closer to a spheroid shape than a bicone shape (spheroid $\gamma = 0.52$ and bicone $\gamma = 0.26$).

From the definition of the parameters, the spindle length (*L*) can be expressed as

$$L^3 = \frac{M}{D\alpha^2\gamma}, \qquad \text{(Equation 1)}$$

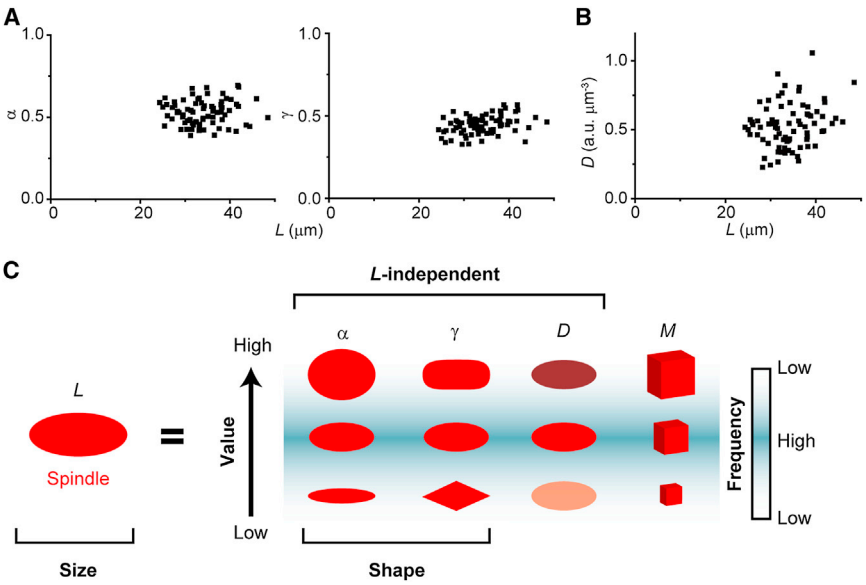

Figure 2. Spindle Length Dependency of Spindle Shape and MT Density

(A) Relationship between spindle shape (α [aspect ratio] and γ) and spindle length (L) (n = 78 spindles).

(B) Relationship between MT density (D) and spindle length (L) (n = 78 spindles).

(C) Schematic illustration for the parameters in Equation 1. The spindle size L is defined by four parameters: α (aspect ratio), γ, D (MT density), and M (amount of MTs). Although the values of these parameters vary among spindles, α, γ, and D are independent of L.

See also Figures S1B, S1C, and Table S2.

where D is the MT density in the spindle defined by M/V (D = 0.53 ± 0.16 arbitrary units (a.u.)/μm^3 [mean ± SD]). We found that D and the spindle length were independent of each other (Figure 2B; Pearson correlation coefficient; r = 0.227 [$p < 0.05$]). Together, these results indicate that the spindle shape (α and γ) and the MT density (D) are independent of the size of intact metaphase spindles that self-organize in *Xenopus* egg extracts. Thus, Equation 1 allows us to evaluate the relationship between the spindle length and the amount of MTs (Figure 2C).

A Decrease or Increase in the Amount of MTs Dynamically Alters the Spindle Size

Because D, α, and γ are nearly independent of L, Equation 1 implies that the change in the amount of MTs (M) largely affects the spindle size. For example, if the value of M is reduced by any perturbations without changes in D, α, and γ, the spindle L, i.e., the spindle size, will become smaller. Therefore, to ascertain the regulation of spindle size by the amount of MTs, we physically reduced the amount of MTs under a microscope. We carefully inserted a pair of glass microneedles near the spindle equator and then separated the spindle into two fragments by rapidly moving the microneedles apart in the direction perpendicular to the pole-to-pole axis (Figure S2A; Movie S1). The manipulation to cut the spindle was completed within ~10 s. Although the chromosomes were divided into two groups, they occasionally detached from the spindle fragment, which resulted in disorganization (Figure S2B).

Each fragment was largely deformed by the manipulation but recovered to the original shape within ~5 min (Figure 3A). After the amount of MTs (M) of each fragment immediately decreased to approximately one-third of the original value, the value of M was maintained nearly constant for ~20 min (Figures 3B and 3C; M = [0.24 ± 0.12] × 10^4 a.u. and [0.074 ± 0.058] × 10^4 a.u. before and after cutting [mean ± SD, n = 10 original spindles and n = 20 fragments]). Accompanied by the reduction of M, each fragment became smaller than the original spindle and did not recover over ~20 min after cutting (Figure 3B; L = 34.1 ± 3.9 μm and 27.1 ± 4.3 μm, W = 16.4 ± 2.2 μm and 12.1 ± 2.7 μm, V = [4.6 ± 1.6] × 10^3 μm^3 and [1.9 ± 1.0] × 10^3 μm^3 before and after cutting, respectively [mean ± SD, n = 10 original spindles and n = 20 fragments]). A relationship between L and M similar to that observed for the original spindles was realized even in the divided spindles with a smaller amount of MTs (Figure 3C). The spindle shape (α and γ) did not change because of cutting (Figures 3B and S3A–S3C; α = 0.48 ± 0.05 and 0.45 ± 0.11, γ = 0.48 ± 0.03 and 0.46 ± 0.09 before and after cutting, respectively [mean ± SD, n = 10 original spindles and n = 20 fragments]). Although the MT density (D) decreased slightly after cutting (Figures 3B, 3D, and S3C; D = 0.50 ± 0.16 and 0.37 ± 0.13 before and after cutting, respectively [mean ± SD, n = 10 original spindles and n = 20 fragments], $p < 0.01$), the extent of change in D (~25%) was lower than that in M (~70%). On the basis of Equation 1, these results indicate that the decrease in spindle length largely corresponds to that in M.

Next, we mechanically manipulated two spindle fragments to contact each other to double the value of M (Figure 4A). Within ~15 min after contact, the fragments gradually fused and became one normal bipolar spindle, which was similar to the process previously observed for the fusion of two normal spindles (Movie S2; Gatlin et al., 2009). The responses of spindle size and shape in the fusion experiment, which represented a more moderate perturbation than the cutting, also followed Equation 1. The value of M for the fused spindle was larger than that of each fragment (Figures 4B and 4C; M = [0.069 ± 0.056] × 10^4 a.u. and [0.18 ± 0.094] × 10^4 a.u. before and after fusion, respectively [mean ± SD, n = 18 fragments and n = 9 fused spindles]). During the process of fusion, the value of M once became larger than the sum of the values of the two fragments. Then, the spindle became larger than each fragment after the fusion was completed (L = 26.2 ± 3.4 μm and 29.9 ± 3.8 μm, W = 12.0 ± 2.8 μm and 16.9 ± 3.9 μm, V = [1.8 ± 1.0] × 10^3 μm^3 and [4.3 ± 2.4] × 10^3 μm^3 before and after fusion [mean ± SD, n = 18 fragments and n = 9 fused spindles]). γ did not change throughout the fusion, whereas the aspect ratio and MT density slightly increased (Figures 4B, 4D, and S3D–S3F; γ = 0.46 ± 0.09 and 0.47 ± 0.04, α = 0.46 ± 0.11 and 0.57 ± 0.15 [$p < 0.01$],

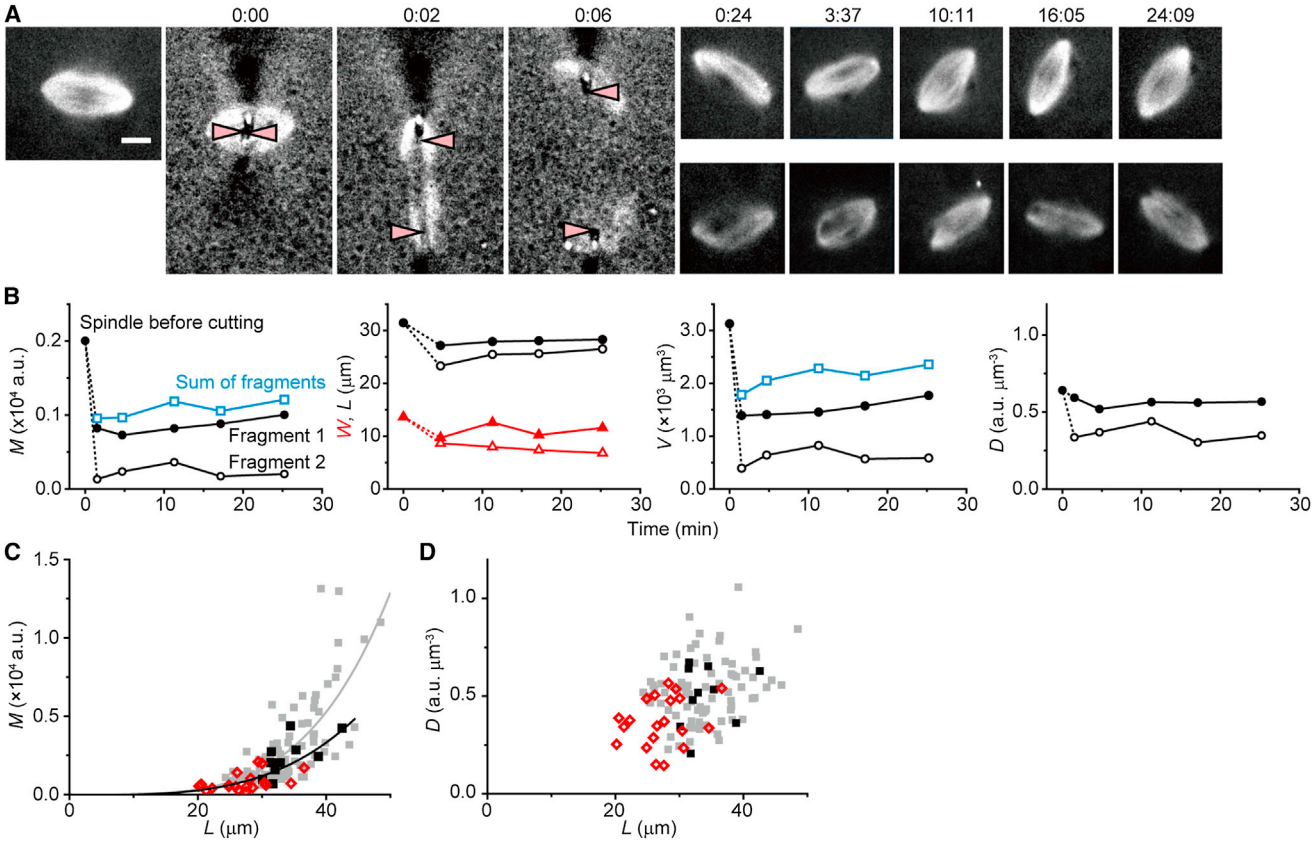

Figure 3. A Decrease in the Amount of MTs Decreases the Spindle Length

(A) Fluorescence images of a spindle and its fragments before, during, and after it was cut into two halves, in which tubulins were labeled with a fluorescent dye. Needle positions are shown by arrowheads. Numbers on the top show the time (min:s) from the moment the spindle was cut. Images before and after cutting show the sum projection of the image stack. The scale bar represents 10 μm.

(B) Time courses of parameters before, during, and after the cutting. Blue open squares for *M* and *V* indicate the sum of the values of two fragments.

(C) Relationship between spindle length (*L*) and the amount of MTs (*M*) before and after cutting (black solid squares [n = 10 spindles] and red open diamonds [n = 20 fragments], respectively; a black solid curve indicates the best fit). Gray solid squares show the relationship for the observed spindles as a control (n = 78 spindles; a gray solid curve indicates the best fit).

(D) Relationship between spindle length (*L*) and MT density (*D*) before and after cutting (black solid squares [n = 10 spindles] and red open diamonds [n = 20 fragments], respectively). Gray solid squares show the relationship for the observed spindles as a control (n = 78 spindles).

See also Figures S2 and S3A–S3C, and Movie S1.

D = 0.36 ± 0.13 and 0.43 ± 0.14 [$p < 0.01$] before and after fusion [mean ± SD, n = 18 fragments and n = 9 fused spindles]). In spite of these changes, the correlation between *L* and *M* of the original spindles was conserved after fusion and after cutting (Figure 4C), indicating that the change in the spindle size corresponds to the change in the amount of MTs.

In this study, we showed that each spindle kept an intrinsic size stably in spite of the variations in the ensemble of many spindles (Figure 1C). Although we still do not fully understand what determines the intrinsic size, our results show that the intrinsic size is not determined solely by the molecular composition around the spindle, because the size was changed after cutting or fusion under the same cytosol. Because the number of chromosomes changed after cutting and fusion, and several reports have shown a correlation between the amount of chromatin and the spindle size (Brown et al., 2007; Dinarina et al., 2009; Gatlin et al., 2009; Loughlin et al., 2011), it is possible that the changes in the number of chromosomes affect the amount of MTs and the spindle size. Another expectation is that in *Xenopus* egg extracts, MT-dependent MT nucleation occurs (Petry et al., 2013), so the amount of MTs at a certain moment might determine the subsequent amount of MTs in the spindle. This expectation is supported by the result that the amount of MTs within the fragment did not change significantly with time after cutting. It should also be noted that the MT density was largely distributed among individual spindles (Figure 2B) even though it was independent of the spindle size. A difference in the number of chromosomes and/or inhomogeneity of cytosol might affect the variations in MT density.

The spindle size changed according to the changes in the amount of MTs induced by cutting or fusion, whereas the spindle shape and MT density remained constant or changed slightly (Figure 4E). Although the spindle shape and the MT density were greatly changed by deformation during the experiment,

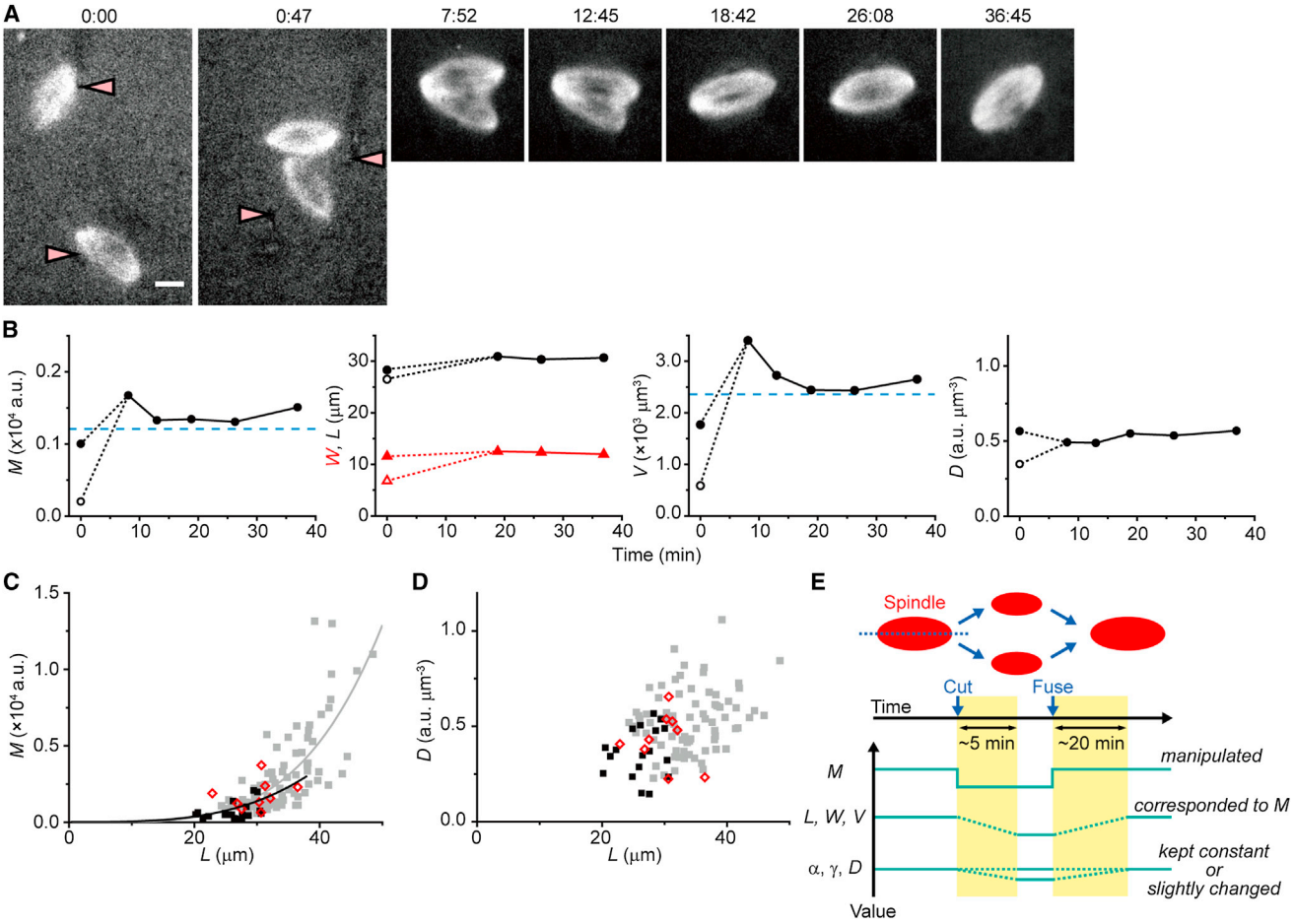

Figure 4. An Increase in the Amount of MTs Increases the Spindle Length

(A) Fluorescence images obtained by 3D observation show how the two spindle fragments were fused. Needle positions are shown by arrowheads. Numbers on the top show the time (min:s) from the moment the fragments began to move. Images after contact represent the sum projection of the image stack. Scale bar: 10 μm.

(B) Time courses of parameters during fusion of two fragments. Blue dashed lines indicate the sum of values of two fragments at time 0.

(C) Relationship between the spindle length (*L*) and the amount of MTs (*M*) before and after fusion (black solid squares [n = 18 fragments] and red open diamonds [n = 9 fused spindles], respectively; a black solid curve indicates the best fit). Gray solid squares show the relationship for the observed spindles as a control (n = 78 spindles, the gray solid curve indicates the best fit).

(D) Relationship between spindle length (*L*) and MT density (*D*) before (black solid squares, n = 18 fragments) and after fusion (red open diamonds, n = 9 fused spindles). Gray solid squares show the relationship for the observed spindles as a control (n = 78 spindles).

(E) Schematic representation showing the changes in the parameters in the cutting and fusion experiments.

See also Figures S3D–S3F and Movie S2.

especially after cutting, they immediately recovered to near the original parameter values (Figures 3A and 3B). According to Equation 1, this result indicates that the dynamic and fast recovery of the spindle shape and MT density contributes to the adjustment of spindle size to the amount of MTs. Because the spindle shape (α and γ) and MT density (*D*) are regulated by molecular motors and MT-associated proteins, probing how these molecules determine and dynamically regulate the spindle shape and MT density could be the key to determine the control mechanism for spindle size.

In contrast to previous models that examined the kinetics of molecular motors and MTs obtained by changing the molecular composition in the cytosol (Burbank et al., 2007; Goshima et al., 2005; Loughlin et al., 2011; Reber et al., 2013), our model reveals the conserved quantities that characterize the spindle structure by using mechanical perturbations without changing the molecular composition in the cytosol. Therefore, the previous models and our model complement each other. The equation we obtained will provide a guideline for examining the mechanisms controlling spindle size and shape.

EXPERIMENTAL PROCEDURES

Spindle Assembly in *Xenopus* Egg Extracts

Xenopus egg extracts were prepared as described previously (Desai et al., 1999). Meiotic spindles self-organized in the extract with the addition of

demembranated *Xenopus* sperm nuclei. All experiments were conducted at 20°C ± 2°C. All experimental procedures conformed to the "Guidelines for Proper Conduct of Animal Experiments" approved by the Science Council of Japan, and were performed according to the regulations for animal experimentation at Waseda University.

Micromanipulation of Spindles

Glass microneedles were fabricated by pulling glass rods (G1000; Narishige) using a capillary puller (PC-10; Narishige). The movement of the needles was manually controlled by two micromanipulators (MHW-3; Narishige).

The egg extract containing meiotic spindles was transferred to a siliconized coverslip (custom-ordered; Matsunami Glass) coated with Pluronic F-127 as described previously (Gatlin et al., 2010). The extract was covered with mineral oil (M-5310; Sigma-Aldrich) to prevent evaporation (Tirnauer et al., 2004).

Microscopy and Imaging Analyses

A fluorescence image of fluorescent-dye-labeled tubulin and a bright-field image of the needle were acquired using a Hamamatsu ORCA AG cooled charge-coupled device (CCD) camera (Hamamatsu Photonics K. K.) or an electron multiplying charge-coupled device (EM-CCD) camera (iXon EM+; Andor Technology) mounted on an inverted microscope (IX 71 or IX 70; Olympus) with an 40 × UplanFLN lens (0.75 NA; Olympus) or 60 × UPlanSApo lens (1.35 NA; Olympus [for 3D scanning]). A confocal scanner unit (CSU10; Yokogawa) was used for 3D image scanning. Image acquisition was performed using Metamorph (Molecular Devices) or Andor iQ (Andor Technology). To visualize the spindles, tubulin labeled with tetramethylrhodamine (Sigma-Aldrich) or Alexa-488 (Sigma-Aldrich) (Hyman et al., 1991) was added (~20 μg ml^{-1}) to the extracts. Images were processed using a median filter to remove background noise. The spindle width (*W*) and length (*L*) were determined using ImageJ (National Institutes of Health). The volume of the spindle estimated by the 2D observation was given by

$$V = 2\pi \frac{R_1 S_1 + R_2 S_2}{2}$$

where R_i (i = 1, 2) represents the distance of the center of mass for each half of the 2D spindle image from the pole-to-pole axis, and S_i (i = 1, 2) represents the area of each half of the spindle. Pearson correlation coefficients were calculated using Origin 8.1 (OriginLab). The statistical significance of the data was confirmed by a paired two-tailed Student's t test in Origin 8.1.

3D Scanning

We doubly labeled the spindle MTs with two types of fluorescent dyes. Alexa-488-labeled tubulin was used to detect the spindles, and tetramethylrhodamine-labeled tubulin was used for 3D scanning (0.5 μm per frame) and to quantitatively obtain 3D images of the spindle. 3D scanning was completed within ~25 s. Then, the obtained 3D data were deconvolved using deconvolution software (Huygens Essential, version 4.1.0p8; Scientific Volume Imaging) that utilized the classic maximum-likelihood estimation algorithm to precisely measure the volume of the spindle. Maximum-intensity projection rendering was performed using Huygens Essential.

We defined a voxel (74 × 74 × 500 nm^3) as the part of the spindle in which the fluorescence intensity was at least 1.5-fold higher than that of the cytoplasm (FI_{Cyto}). Thus, the threshold for the fluorescence intensity of the spindle MTs (FI_{Th}) is given by

$$FI_{Th} = 1.5\, FI_{Cyto}$$

The volume of the spindle (*V*) is given by

$$V = v^* \sum_{i}^{FI_i > FI_{Th}} 1,$$

where *i* is the index of voxels in the 3D data, FI_i is the fluorescence intensity of the *i*-th voxel, and *v* is the volume of each voxel. The total amount of MTs in the spindle (*M*) was defined as the total *FI* of the spindle given by

$$M = \sum_{i}^{FI_i > FI_{Th}} \left(FI_i - FI_{cyto}\right)$$

MT density (*D*) was defined as the average *FI* density in the spindle given by

$$D = \frac{M}{V}$$

Photobleaching was calibrated using a previously reported equation that describes fluorescence recovery (Salmon et al., 1984); that is, the recovery of fluorescence intensity of each voxel at time *t* caused by remodeling of the spindle after the first 3D scanning (FI_t) is given by

$$FI_t = FI_0 + (FI_\infty - FI_0)\left(1 - e^{-\frac{t}{\tau}}\right)$$

where FI_0 is the fluorescence intensity immediately after the first scan; i.e., just after photobleaching occurs in the first scan. FI_∞ is the fully recovered fluorescence intensity after photobleaching. The recovery time, τ, was experimentally determined from the recovery curve, which was obtained by measuring the FI_t at various time moments, *t*, during the second scan. To minimize the contribution of photobleaching, only one data point of FI_t was used to obtain the relaxation time, τ, characteristic of the recovery curve. The obtained value of τ was ~63 s (n = 11 spindles).

SUPPLEMENTAL INFORMATION

Supplemental Information includes Extended Experimental Procedures, three figures, two tables, and two movies and can be found with this article online at http://dx.doi.org/10.1016/j.celrep.2013.09.021.

AUTHOR CONTRIBUTIONS

J.T. conducted the experiments; J.T., T.I., K.S., and S.I. designed the experiments and wrote the manuscript; and Y.S. and T.M.K. provided advice on the experiments, the analyses, and the manuscript.

ACKNOWLEDGMENTS

This work was supported by the Research Fellowship for Young Scientists (DC1; to J.T. and K.S.), a Grant-in-Aid for Scientific Research (C; to T.I.), and the Grants-in-Aid for Specially Promoted Research and Scientific Research (S; to S.I.) from the Ministry of Education, Culture, Sports, Science and Technology of Japan. T.M.K. is grateful to the NIH/NIGMS (GM65933) for funding. Y.S. is grateful for support from JST PRESTO.

Received: July 31, 2013
Revised: September 18, 2013
Accepted: September 20, 2013
Published: October 10, 2013

REFERENCES

Andersen, S.S. (2000). Spindle assembly and the art of regulating microtubule dynamics by MAPs and Stathmin/Op18. Trends Cell Biol. *10*, 261–267.

Brown, K.S., Blower, M.D., Maresca, T.J., Grammer, T.C., Harland, R.M., and Heald, R. (2007). Xenopus tropicalis egg extracts provide insight into scaling of the mitotic spindle. J. Cell Biol. *176*, 765–770.

Brust-Mascher, I., Sommi, P., Cheerambathur, D.K., and Scholey, J.M. (2009). Kinesin-5-dependent poleward flux and spindle length control in Drosophila embryo mitosis. Mol. Biol. Cell *20*, 1749–1762.

Budde, P.P., Kumagai, A., Dunphy, W.G., and Heald, R. (2001). Regulation of Op18 during spindle assembly in Xenopus egg extracts. J. Cell Biol. *153*, 149–158.

Burbank, K.S., Mitchison, T.J., and Fisher, D.S. (2007). Slide-and-cluster models for spindle assembly. Curr. Biol. *17*, 1373–1383.

Desai, A., Murray, A., Mitchison, T.J., and Walczak, C.E. (1999). The use of Xenopus egg extracts to study mitotic spindle assembly and function in vitro. Methods Cell Biol. *61*, 385–412.

Dinarina, A., Pugieux, C., Corral, M.M., Loose, M., Spatz, J., Karsenti, E., and Nédélec, F. (2009). Chromatin shapes the mitotic spindle. Cell *138*, 502–513.

Dumont, S., and Mitchison, T.J. (2009). Compression regulates mitotic spindle length by a mechanochemical switch at the poles. Curr. Biol. *19*, 1086–1095.

Gaetz, J., and Kapoor, T.M. (2004). Dynein/dynactin regulate metaphase spindle length by targeting depolymerizing activities to spindle poles. J. Cell Biol. *166*, 465–471.

Gaetz, J., Gueroui, Z., Libchaber, A., and Kapoor, T.M. (2006). Examining how the spatial organization of chromatin signals influences metaphase spindle assembly. Nat. Cell Biol. *8*, 924–932.

Gatlin, J.C., Matov, A., Groen, A.C., Needleman, D.J., Maresca, T.J., Danuser, G., Mitchison, T.J., and Salmon, E.D. (2009). Spindle fusion requires dynein-mediated sliding of oppositely oriented microtubules. Curr. Biol. *19*, 287–296.

Gatlin, J.C., Matov, A., Danuser, G., Mitchison, T.J., and Salmon, E.D. (2010). Directly probing the mechanical properties of the spindle and its matrix. J. Cell Biol. *188*, 481–489.

Goshima, G., Wollman, R., Stuurman, N., Scholey, J.M., and Vale, R.D. (2005). Length control of the metaphase spindle. Curr. Biol. *15*, 1979–1988.

Hara, Y., and Kimura, A. (2009). Cell-size-dependent spindle elongation in the Caenorhabditis elegans early embryo. Curr. Biol. *19*, 1549–1554.

Hara, Y., and Kimura, A. (2013). An allometric relationship between mitotic spindle width, spindle length, and ploidy in Caenorhabditis elegans embryos. Mol. Biol. Cell *24*, 1411–1419.

Heald, R., Tournebize, R., Blank, T., Sandaltzopoulos, R., Becker, P., Hyman, A., and Karsenti, E. (1996). Self-organization of microtubules into bipolar spindles around artificial chromosomes in Xenopus egg extracts. Nature *382*, 420–425.

Houghtaling, B.R., Yang, G., Matov, A., Danuser, G., and Kapoor, T.M. (2009). Op18 reveals the contribution of nonkinetochore microtubules to the dynamic organization of the vertebrate meiotic spindle. Proc. Natl. Acad. Sci. USA *106*, 15338–15343.

Hyman, A., Drechsel, D., Kellogg, D., Salser, S., Sawin, K., Steffen, P., Wordeman, L., and Mitchison, T. (1991). Preparation of modified tubulins. Methods Enzymol. *196*, 478–485.

Itabashi, T., Takagi, J., Shimamoto, Y., Onoe, H., Kuwana, K., Shimoyama, I., Gaetz, J., Kapoor, T.M., and Ishiwata, S. (2009). Probing the mechanical architecture of the vertebrate meiotic spindle. Nat. Methods *6*, 167–172.

Kaláb, P., Pralle, A., Isacoff, E.Y., Heald, R., and Weis, K. (2006). Analysis of a RanGTP-regulated gradient in mitotic somatic cells. Nature *440*, 697–701.

Loughlin, R., Wilbur, J.D., McNally, F.J., Nédélec, F.J., and Heald, R. (2011). Katanin contributes to interspecies spindle length scaling in Xenopus. Cell *147*, 1397–1407.

McNally, K., Audhya, A., Oegema, K., and McNally, F.J. (2006). Katanin controls mitotic and meiotic spindle length. J. Cell Biol. *175*, 881–891.

Merdes, A., Ramyar, K., Vechio, J.D., and Cleveland, D.W. (1996). A complex of NuMA and cytoplasmic dynein is essential for mitotic spindle assembly. Cell *87*, 447–458.

Mitchison, T.J., Maddox, P., Gaetz, J., Groen, A., Shirasu, M., Desai, A., Salmon, E.D., and Kapoor, T.M. (2005). Roles of polymerization dynamics, opposed motors, and a tensile element in governing the length of Xenopus extract meiotic spindles. Mol. Biol. Cell *16*, 3064–3076.

Oguchi, Y., Uchimura, S., Ohki, T., Mikhailenko, S.V., and Ishiwata, S. (2011). The bidirectional depolymerizer MCAK generates force by disassembling both microtubule ends. Nat. Cell Biol. *13*, 846–852.

Ohi, R., Burbank, K., Liu, Q., and Mitchison, T.J. (2007). Nonredundant functions of Kinesin-13s during meiotic spindle assembly. Curr. Biol. *17*, 953–959.

Petry, S., Groen, A.C., Ishihara, K., Mitchison, T.J., and Vale, R.D. (2013). Branching microtubule nucleation in Xenopus egg extracts mediated by augmin and TPX2. Cell *152*, 768–777.

Reber, S.B., Baumgart, J., Widlund, P.O., Pozniakovsky, A., Howard, J., Hyman, A.A., and Jülicher, F. (2013). XMAP215 activity sets spindle length by controlling the total mass of spindle microtubules. Nat. Cell Biol. *15*, 1116–1122.

Rubinstein, B., Larripa, K., Sommi, P., and Mogilner, A. (2009). The elasticity of motor-microtubule bundles and shape of the mitotic spindle. Phys. Biol. *6*, 016005.

Salmon, E.D., Leslie, R.J., Saxton, W.M., Karow, M.L., and McIntosh, J.R. (1984). Spindle microtubule dynamics in sea urchin embryos: analysis using a fluorescein-labeled tubulin and measurements of fluorescence redistribution after laser photobleaching. J. Cell Biol. *99*, 2165–2174.

Sawin, K.E., LeGuellec, K., Philippe, M., and Mitchison, T.J. (1992). Mitotic spindle organization by a plus-end-directed microtubule motor. Nature *359*, 540–543.

Shimamoto, Y., Maeda, Y.T., Ishiwata, S., Libchaber, A.J., and Kapoor, T.M. (2011). Insights into the micromechanical properties of the metaphase spindle. Cell *145*, 1062–1074.

Tirnauer, J.S., Salmon, E.D., and Mitchison, T.J. (2004). Microtubule plus-end dynamics in Xenopus egg extract spindles. Mol. Biol. Cell *15*, 1776–1784.

Vernos, I., Raats, J., Hirano, T., Heasman, J., Karsenti, E., and Wylie, C. (1995). Xklp1, a chromosomal Xenopus kinesin-like protein essential for spindle organization and chromosome positioning. Cell *81*, 117–127.

Wollman, R., Civelekoglu-Scholey, G., Scholey, J.M., and Mogilner, A. (2008). Reverse engineering of force integration during mitosis in the Drosophila embryo. Mol. Syst. Biol. *4*, 195.

Wühr, M., Chen, Y., Dumont, S., Groen, A.C., Needleman, D.J., Salic, A., and Mitchison, T.J. (2008). Evidence for an upper limit to mitotic spindle length. Curr. Biol. *18*, 1256–1261.